GA–A25229

FINAL REPORT ON THE OFES ELM MILESTONE FOR FY05

by
D.P. BRENNAN, E.D. HELD, S.E. KRUGER, A.Y. PANKIN,
D.D. SCHNACK, AND C.R. SOVINEC

APRIL 2006

GENERAL ATOMICS

DISCLAIMER

GA–A25229

FINAL REPORT ON THE OFES ELM MILESTONE FOR FY05

by
D.P. BRENNAN,[*,+] E.D. HELD,[†] S.E. KRUGER,[‡] A.Y. PANKIN,[#]
D.D. SCHNACK,[#] AND C.R. SOVINEC[¶]

[*]Massachusetts Institute of Technology, Cambridge, Massachusetts, USA
[+]General Atomics, San Diego, California, USA
[†]Utah State University, Logan, Utah, USA
[‡]Tech-X Corporation, Boulder, Colorado, USA
[#]Science Applications International Corporation, San Diego, California, USA
[¶]University of Wisconsin, Madison, Wisconsin, USA

**Work supported by
the U.S. Department of Energy under
DE-FG02-95ER54309, and DE-FG02-92ER54139**

**GENERAL ATOMICS PROJECT 03726
APRIL 2006**

GENERAL ATOMICS

EXECUTIVE SUMMARY

This document reports the successful completion of the OFES Theory Milestone for FY05; namely, *Perform parametric studies to better understand the edge physics regimes of laboratory experiments. Simulate at increased resolution (up to 20 toroidal modes), with density evolution, late into the nonlinear phase and compare results from different types of edge modes. Simulate a single case including a study of heat deposition on nearby material walls.*

The linear stability properties and nonlinear evolution of Edge Localized Modes (ELMs) in tokamak plasmas are investigated through numerical computation. Data from the DIII-D device at General Atomics (http://fusion.gat.com/diii-d/) is used for the magnetohydrodynamic (MHD) equilibria, but edge parameters are varied to reveal important physical effects. The equilibrium with very low magnetic shear produces an unstable spectrum that is somewhat insensitive to dissipation coefficient values. Here, linear growth rates from the non-ideal NIMROD code (http://nimrodteam.org) agree reasonably well with ideal, i.e. non-dissipative, results from the GATO global linear stability code at low toroidal mode number (n) and with ideal results from the ELITE edge linear stability code at moderate to high toroidal mode number. Linear studies with a more realistic sequence of MHD equilibria (based on DIII-D discharge 86166) produce more significant discrepancies between the ideal and non-ideal calculations. The maximum growth rate for the ideal computations occurs at toroidal mode index $n = 10$, whereas growth rates in the non-ideal computations continue to increase with n unless strong anisotropic thermal conduction is included. Recent modeling advances allow drift effects associated with the Hall electric field and gyroviscosity to be considered. A stabilizing effect can be observed in the preliminary results, but while the distortion in mode structure is readily apparent at $n = 40$, the growth rate is only 13% less than the non-ideal MHD result. Computations performed with a non-local kinetic closure for parallel electron thermal conduction that is valid over all collisionality regimes identify thermal diffusivity ratios of $\chi_{\parallel}/\chi_{\perp} \sim 10^{7} - 10^{8}$ as appropriate when using collisional heat flux modeling for these modes. Adding significant parallel viscosity proves to have little effect.

Nonlinear ELM computations solve the resistive MHD model with toroidal resolution $0 \le n \le 21$, including anisotropic thermal conduction, temperature-dependent resistivity, and number density evolution. The computations are based on a realistic equilibrium with high pedestal temperature from the linear study. When the simulated ELM grows to appreciable amplitude, ribbon-like thermal structures extend from the separatrix to the

wall as the spectrum broadens about a peak at $n = 13$. Analysis of the results finds the heat flux on the wall to be very nonuniform with greatest intensity occurring in spots on the top and bottom of the chamber. Net thermal energy loss occurs on a time-scale of 100 μs, and the instantaneous loss rate exceeds 1 GW.

1. INTRODUCTION

With recent advances in computer hardware and numerical algorithm efficiency, large-scale computational modeling can play an important role in the design and analysis of fusion devices. Among the nations engaged in developing magnetic confinement fusion, the US remains the world leader in plasma simulation. An example of an important fusion problem that is being addressed by this approach is the onset and nonlinear evolution of Edge Localized Modes (ELMs) and their effect on global confinement and first wall performance [1]. These modes shed thermal energy from the edge of the confinement region and, in their most virulent form, release enough energy to be of concern for plasma-facing components of future burning plasma experiments. They may also affect the core plasma through nonlinear mode coupling. During FY05, the NIMROD Team (http://nimrodteam.org) has begun a numerical study of the global dynamics of ELMs in tokamaks. The unique capabilities of our advanced extended-MHD model [2] allow us to simulate ELMs farther into the nonlinear regime than what has been previously achieved.

Previous studies have found the underlying character of ELMs to be an MHD instability described as "peeling-ballooning" [3-5]. The "peeling" component of the instability is the free-energy drive due to the current density gradient, and the "ballooning" component is the free-energy drive due to the pressure gradient. At the edge of the confinement region of tokamaks, poloidal flows reduce energy transport and allow a steep pressure gradient to develop. Through bootstrap-current effects, the strong pressure gradient drives highly localized current density. The pressure and current gradients are also coupled through the MHD equilibrium force-balance, but they affect distinct characteristics in the linearly unstable modes that are excited. An individual ELM will typically display a combination of both sets of characteristics, however.

Our linear stability analysis of a set of tokamak equilibria having varying degrees of peeling and ballooning drive is outlined in Sec. 2. A sequence of nonlinear simulations follow a spectrum of ELMs from the linear stage to finite amplitude, where they become coupled and transport heat beyond the confinement zone and to the wall. These results are presented in Sec. 3. A brief summary and discussion is presented in Sec. 4.

2. LINEAR STABILITY

2.1 BALLOONING-COMPONENT-DOMINANT EQUILIBRIA

A model tokamak equilibrium configuration has been constructed to be robustly unstable, due to low magnetic shear and poloidal shaping, while remaining in the global parameter space of typical DIII-D discharges. The localized edge current density and pressure gradient described in Sec. 1 are clearly evident in the profiles shown in Fig. 1. This ballooning-dominant configuration is relatively easy to resolve radially. Consistent with the MHD theory of ballooning modes, the resistive MHD computations find that growth rates increase monotonically with n. The unfortunate implication is that toroidal resolution in a nonlinear resistive MHD simulation cannot be achieved. Nonetheless, this equilibrium provides a suitable benchmark case for comparing linear results obtained with different numerical approaches.

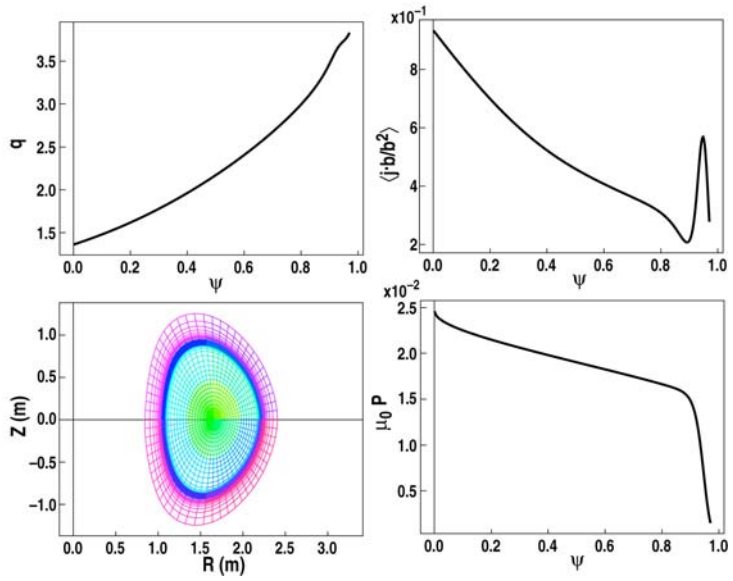

Fig. 1. Safety factor (q), parallel current density ($\mathbf{j}\cdot\mathbf{b}/\mathbf{b}^2$), and pressure profiles for the low-shear equilibrium discussed in Sec. 2.1. The computational mesh of finite elements used for the linear computations is also shown.

The linear results of NIMROD compare favorably with results from the ELITE and GATO [4] codes with eigenfunctions and growth rates that are in reasonable agreement. The growth rates computed by NIMROD with non-ideal MHD depend on the resistivity and viscosity in the vicinity of the mode, as discussed below, but the variation of growth rate with n agrees qualitatively with the GATO and ELITE results, as shown in Fig. 2. Varying the electrical resistivity shaping parameter by three orders of magnitude affects the growth rate values (by less than a factor of 2), but it does not change the spectrum

qualitatively. Here, the magnetic Prandtl number (Pm, the ratio of kinematic viscosity to electrical diffusivity) is held fixed while both the core and surrounding resistivity values are varied. In obtaining the results for this equilibrium, the linear behavior of 22 toroidal modes have been determined with 3 values of resistivity and 3 values of thermal conductivity, for a total of 198 numerical calculations. The results represent the first linear ELM studies to include collisionality and separatrix effects.

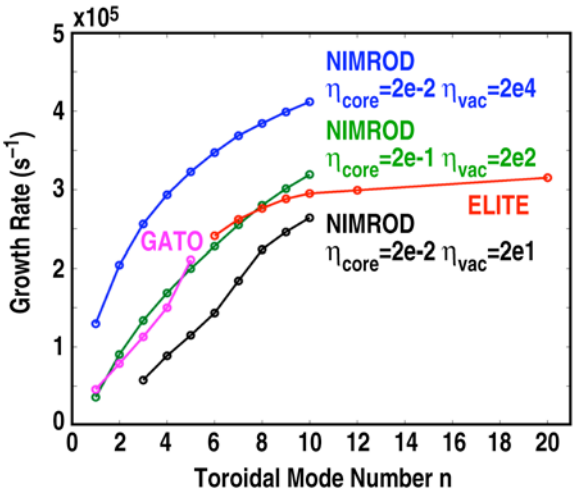

Fig. 2. Linear growth rates for a range of n-values with confinement-region resistivity (η_{core}) and surrounding layer resistivity (η_{vac}) varied show good agreement with ideal MHD codes. Because the eigenfunctions extend into the open-field line region, the growth rates depend on the "vacuum" resistivity, but the changes are less than a factor of 2.

2.2. REALISTIC EQUILIBRIA

Equilibria reconstructed with data from a high-pressure DIII-D discharge that produced ELMs provide the basis of this investigation. The poloidal magnetic field configuration has a single null below the confinement region. The non-dimensional geometric and profile properties are also similar to high performance tokamak operation ("H-mode") in Alcator C-mod (http://www.psfc.mit.edu) and advanced scenarios for ITER (http://www.iter.org). The parallel current density, magnetic winding ratio (or 'safety factor,' q), and pressure profiles for three of the equilibria are shown in Fig. 3. They are parameterized by their edge pedestal temperatures $\left(T_{ped}\right)$ with the 100 eV, 400 eV, and 700 eV profiles shown in the figure. The q-value is above 1 across each profile, which stabilizes the internal ideal kink mode and allows our study to focus on edge-localized modes. The equilibrium with $T_{ped} = 100$ eV does not have any significant gradients in the edge.

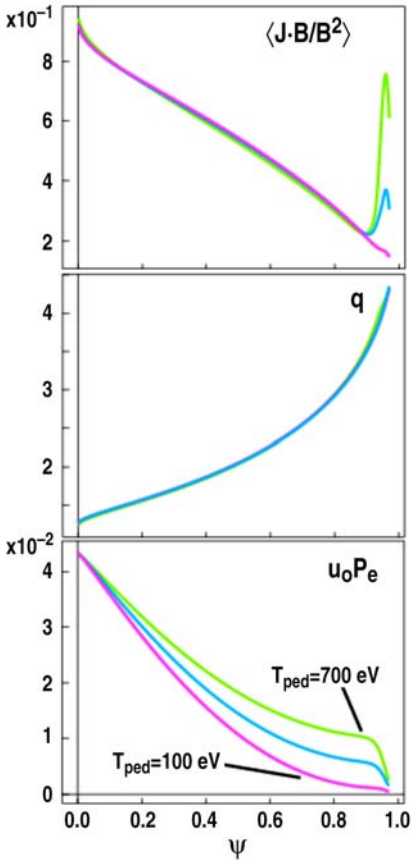

Fig. 3. MHD equilibria representative of DIII-D with successively decreasing pedestal temperature but similar cross sectional shape. The top figure shows the parallel current profiles, the middle figure shows the q-profiles, and the bottom figure shows the pressure for the three pedestal temperatures used in the study.

The linear stability properties of this set of equilibria have been studied with the NIMROD code with the Lundquist number (S) set to 2×10^7. The linear growth rate spectrum with respect to toroidal mode number is shown in Fig. 4 for two of the equilibria. All modes for the $T_{ped} = 400$ eV and 700 eV cases are found to be unstable, and the growth rates of the unstable modes increase with increasing *n*. The $T_{ped} = 700$ eV computation produces large linear growth rates ($\gamma\tau_A = 0.36$, where τ_A is the global Alfvén propagation time) at low Pm-values with the non-ideal model. This indicates that the respective equilibrium is well above the threshold for ideal linear instability, a condition that is unlikely to occur in the actual experiment. The $T_{ped} = 100$ eV equilibrium is near the stability boundary.

Resistive MHD produces growth rates that increase with n for ballooning-dominant equilibria, but high-n ELM fluctuations are not detected in experiments. Conventional wisdom holds that two-fluid effects are stabilizing at large n-values, and this is often cited to explain the observations. We have applied extended MHD modeling [6] to the equilibria shown in Fig. 3 (also see Ref. [5]), and preliminary results for the

$T_{ped} = 400$ eV equilibrium are summarized in Fig. 5. Here we plot the linear growth rate as a function of the toroidal mode number for three different models (MHD, Hall-MHD, and Hall-MHD with gyroviscosity) with and without anisotropic ($\chi_{\|}/\chi_{\perp} = 10^7$) thermal diffusivity. The strongest stabilizing effect is provided by the anisotropic thermal diffusivity, where the ratio of diffusivity coefficients has been determined by computations performed with a non-local kinetic closure for parallel electron thermal conduction that is valid over all collisionality regimes [7]. A linear computation for the $T_{ped} = 700$ eV equilibrium without anisotropic thermal conduction finds only a 13% reduction in growth rate when Hall and gyroviscous effects are included at $n = 40$.

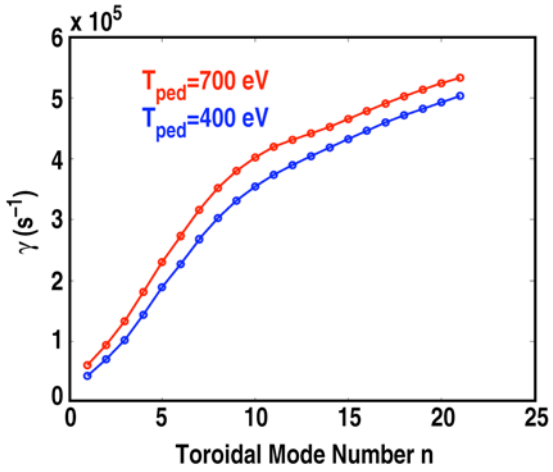

Fig. 4. Linear growth rates as a function of toroidal mode index n for the equilibria with pedestal temperatures of 400 eV (blue trace) and 700 eV (red trace). The 100 eV equilibrium is near the stability threshold.

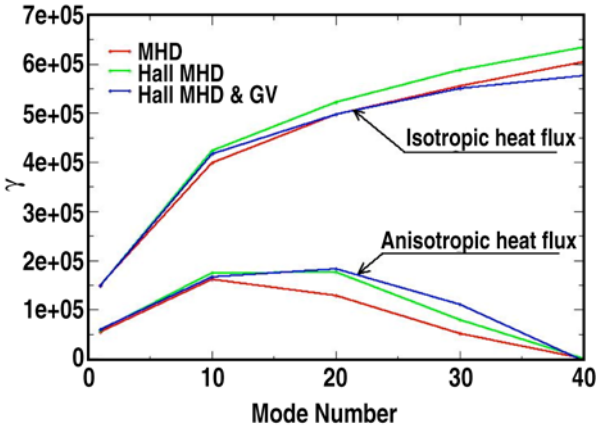

Fig. 5. Linear growth rate as a function of toroidal mode number for the case of 400 eV pedestal temperature, S = 3.7×10^7, Pm = 10^{-3}.

3. NONLINEAR RESISTIVE MHD

Nonlinear, resistive MHD simulations with anisotropic heat conduction have been performed with several of the equilibria discussed above. Here, we present a computation that is based on the $T_{ped} = 700$ eV equilibrium shown in Fig. 3. Small amplitude perturbations in the initial conditions excite unstable ELMs, and the computation follows their evolution well into the nonlinear phase. The electrical resistivity is temperature-dependent (Spitzer resistivity, based on the evolving toroidally averaged temperature). The viscous diffusivity and perpendicular thermal diffusivity are $25\ \mathrm{m}^2/\mathrm{s}$, and the parallel thermal diffusivity is 10^5 times larger. The spatial domain is represented by an appropriately packed 40×72 mesh of biquartic finite elements for the poloidal plane and Fourier components $0 \le n \le 21$ for the toroidal direction.

The temporal evolution of the kinetic energy associated with each of the toroidal Fourier components is shown in Fig. 6. There is a linear growth phase for 0.05 ms $< t <$ 0.1 ms, followed by nonlinear saturation. Only modes in the range $7 \le n \le 19$ exhibit linear growth, as shown in Fig. 7. In contrast to the results shown in Fig. 4, the growth rate spectrum is peaked around $n = 13$. This is attributed to the anisotropic thermal conduction (see Fig. 5), viscous dissipation, and the large current-gradient (peeling component) at the edge of the confinement region in this equilibrium. Numerical convergence tests indicate that while greater resolution is needed to achieve quantitative accuracy, the peaked linear spectrum is qualitatively correct. Other modes may be linearly unstable but grow too slowly to show independent activity before nonlinear coupling becomes significant. Of particular importance is that the nonlinear coupling drives low n-fluctuations (including $n = 1$), in addition to high-n fluctuations, and low-n activity in the edge may excite resonant effects in the core plasma.

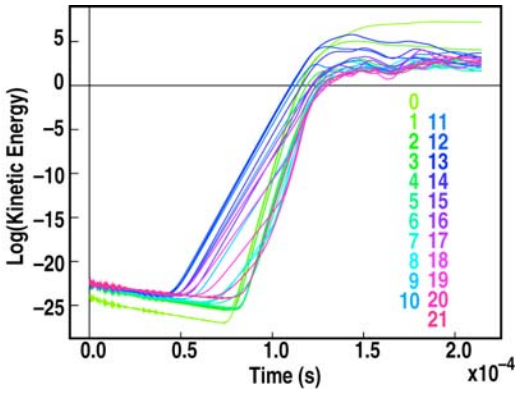

Fig. 6. The evolution of kinetic fluctuation energy (on a logarithmic scale) of each toroidal harmonic shows that the broad linear mode spectrum nonlinearly drives the linearly stable $n = 0$ and $n = 1$ components. They have the largest energies at the end of the simulation.

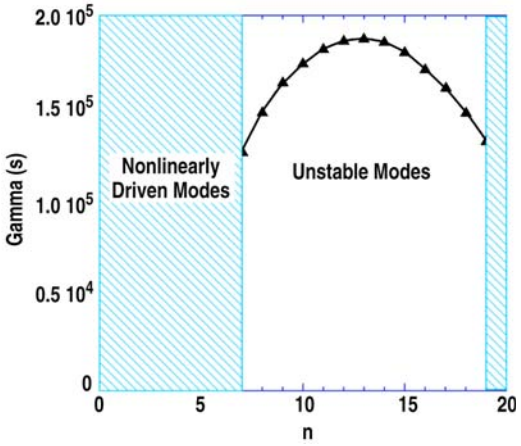

Fig. 7. Linear growth rates measured from the early phase of the nonlinear simulation shows a broad spectrum peaked at $n = 13$. The equilibrium is the same as the $T_{ped} = 700$ eV profile of Fig. 3.

The character of the non-linear behavior of the edge modes in this discharge is summarized in Figs. 8-10, which show several properties of the discharge at selected times during the evolution. The upper right hand section of each of these figures shows color contours of the pressure in the $\phi = 0$ toroidal plane. The blue region represents the cold plasma outside the confinement region. The black overlaid contour is a surface at which the normal component of the convective heat flux ($q_V = \hat{\mathbf{n}} \cdot \mathbf{V} nT$) is computed. (This simulation has a computational domain that extends "self-similarly" beyond the confinement region. The surface at which the heat flux is measured also conforms to the boundary, and the outboard midplane location corresponding to the position of the DIII-D wall.) The lower right hand section contains a Poincaré plot of the magnetic field-line punctures in the $\phi = 0$ toroidal plane. The lower left hand section shows perspective views of pressure contours at four toroidal planes equally spaced around the torus. This displays the three-dimensional structure of the dynamics. The upper left hand section shows color contours of the convective heat flux at the surface indicated by the black contour shown in the upper right hand section. This contour has been "unwrapped" into the poloidal-toroidal plane. Arrows show the relationships between the poloidal locations in this plot and the black contour in the figure to the right. Only the convective heat flux is shown because its contribution to the heat loss is greater than that of the conductive heat loss, in contrast to NIMROD simulation results on plasma disruption due to an internal mode [8].

Figure 8 shows that configuration at $t = 0.115$ ms, the start of the nonlinear phase. Small corrugations are visible in the pressure contours, but the magnetic field-lines trace out nested flux surfaces, and there is no significant loss of heat. Figure 9 shows the configuration at $t = 0.144$ ms, the time of peak amplitude of convective heat flux. Ribbons of plasma pressure now extend beyond the black boundary contour and have eroded a significant portion of the plasma core. The field in the edge has become

stochastic, contributing to heat loss. The convective heat flux appears as bright spots on the boundary surface, primarily near the top and bottom of the chamber. An overall striation pattern in the heat flux deposition is evident. The striation pattern differs in the four major regions: outboard, top, bottom (separatrix), and inboard. The maximum heat flux is localized in the top and bottom regions with greatest concentration in the top region, where the triangularity of the equilibrium is not as strong. Figure 10 shows conditions at the end of the calculation, when the ribbons are retreating back toward the plasma. The mode structure increases in poloidal extent, and the heat flux structure shows little difference between the top region and the upper inboard region. The differences between the upper inboard region and lower inboard region are due to the lower single null configuration of this plasma. These preliminary results suggest that high triangularity would be effective in preventing heat flux from reaching the inboard side. The magnetic field remains stochastic over much of the outer portion of the discharge.

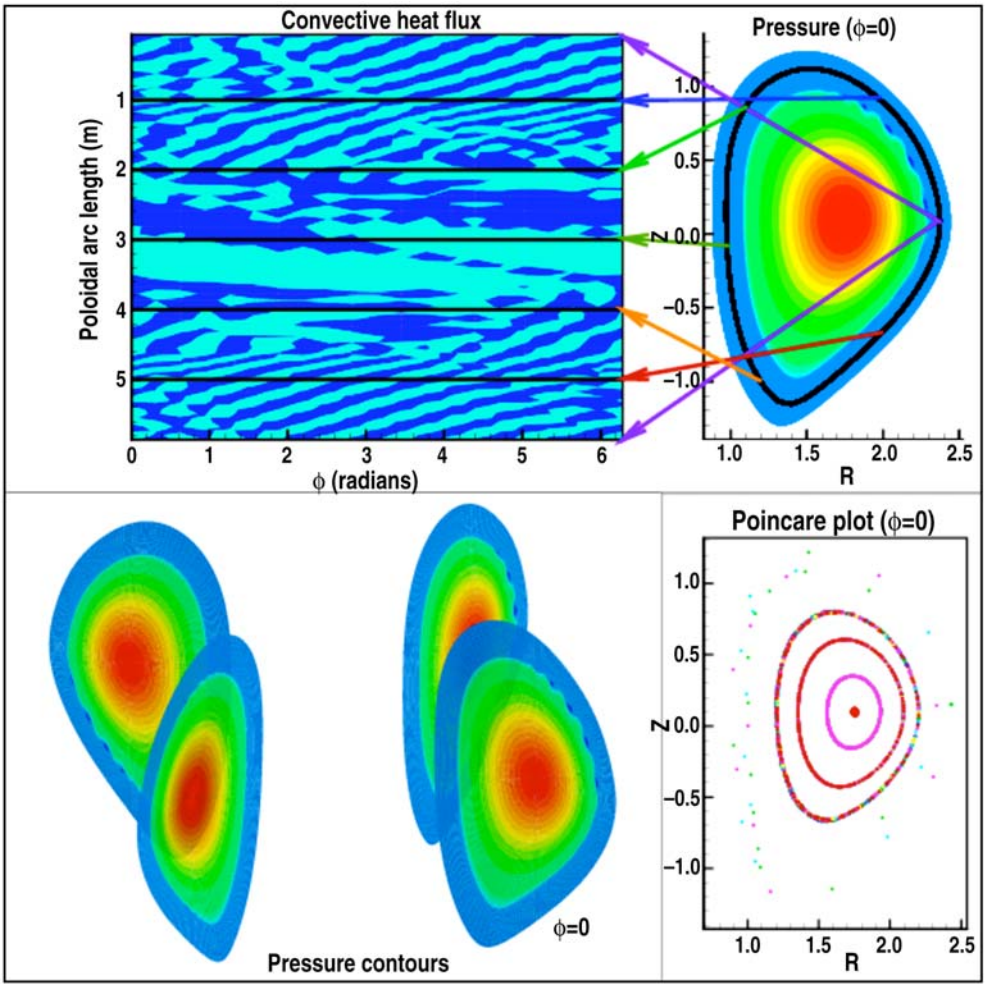

Fig. 8. Convective heat flux as a function of poloidal arc length and toroidal angle is shown, at t = 0.115 ms. Arrows indicate location of the measures of poloidal arc length. The three dimensional structure can be seen by the pressure contours in the lower left corner.

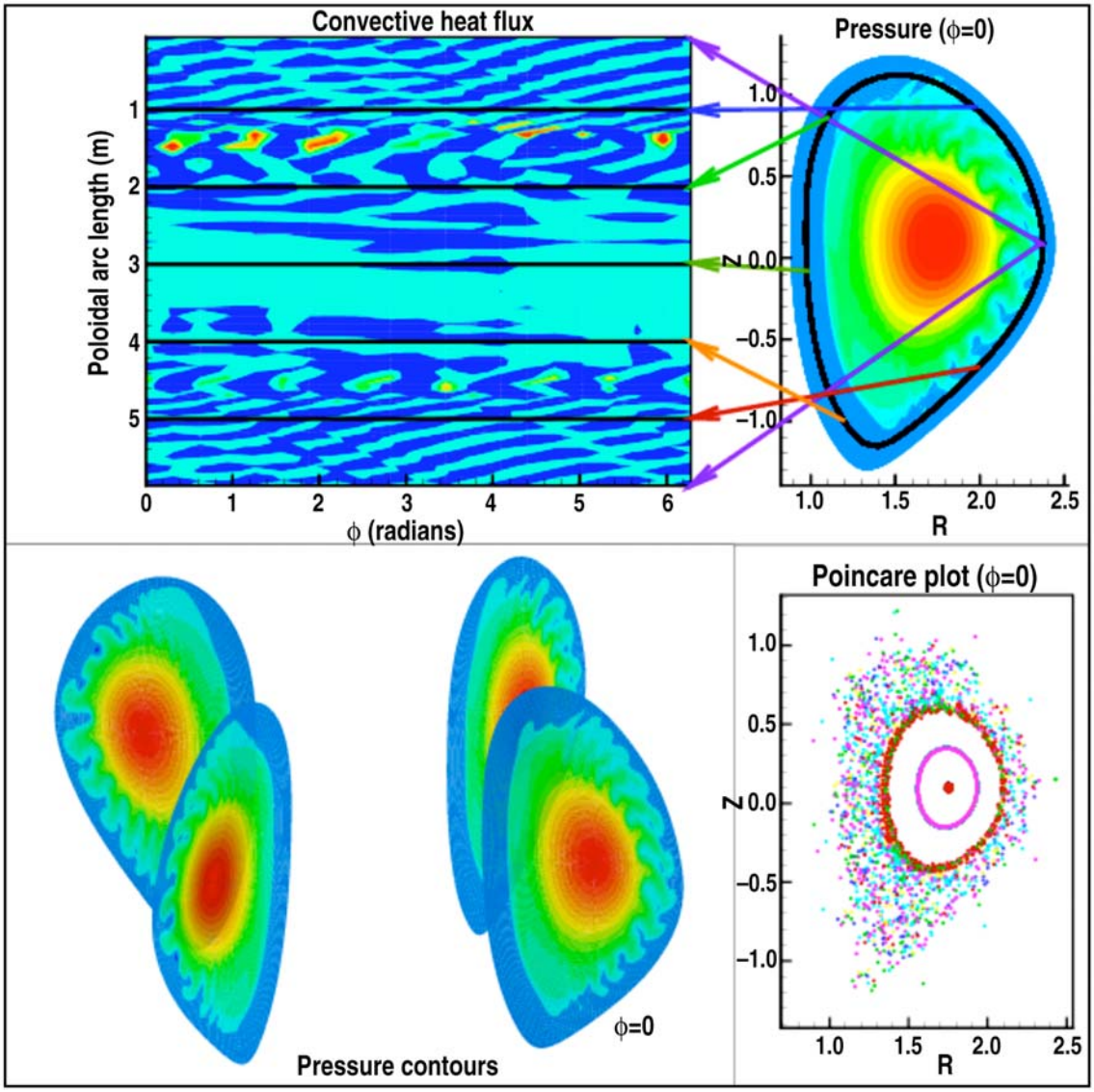

Fig. 9. At t = 0.144 ms, the heat load on the wall is at its peak. The three-dimensional load structure shows complicated structure that has penetrated toward the interior of the plasma.

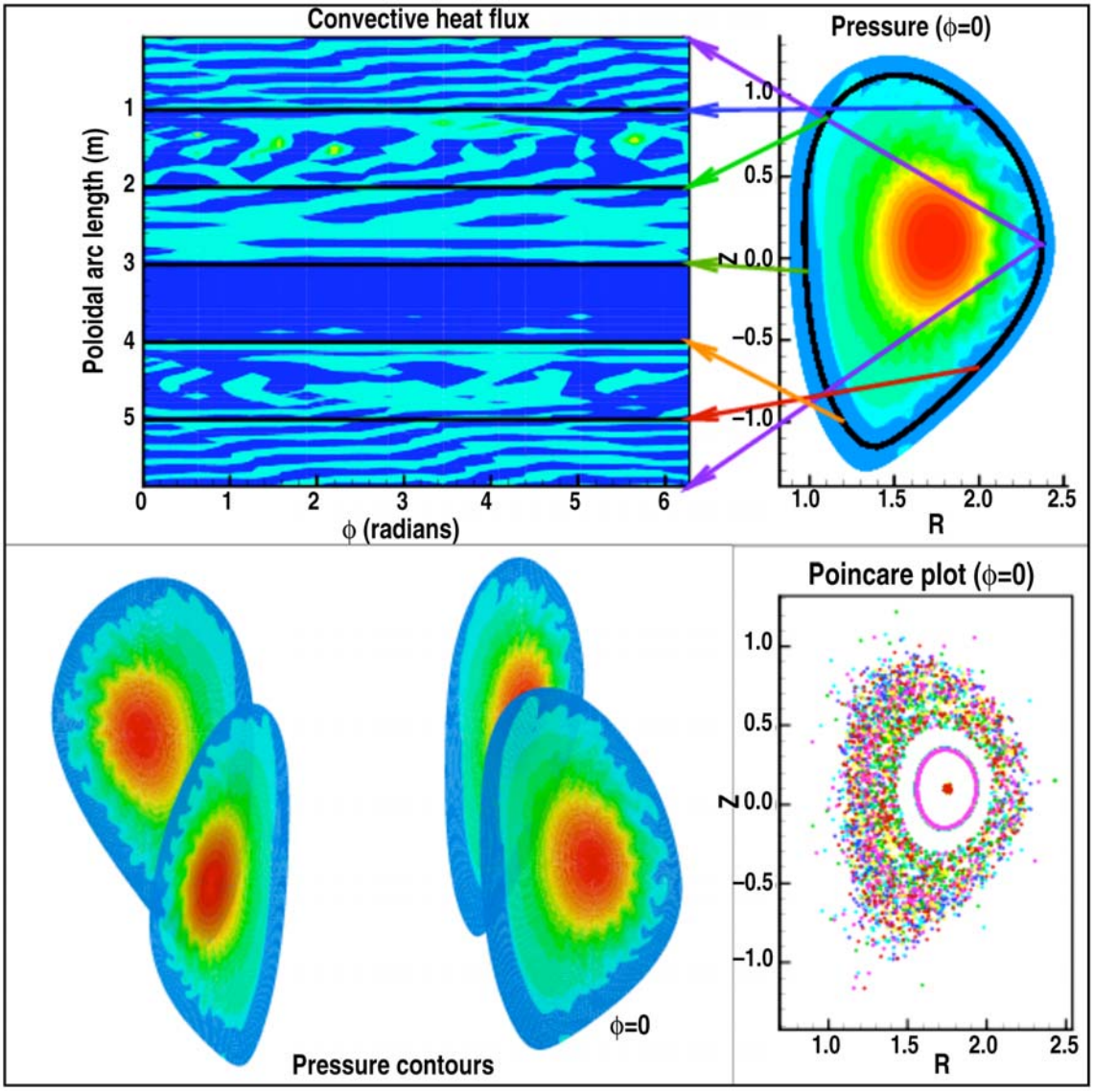

Fig. 10. Near the end of the simulation, the poloidal extent of the mode has increased and the field is almost completely stochastic. The $n = 1$ structure can be seen within the high harmonic structure.

The evolution is more dynamic than what is evident from still figures. An animation of the evolution represented by Figs. 8-10 can be found at:

http://fusion.txcorp.com/~kruger/elma10n_images/elma10n.gif.

The nonlinear evolution of this mode drives a rapid loss of internal energy with approximately 70 kJ $(\sim 10\%)$ of the internal energy being lost within 60 μs, as shown in Fig. 11. Laboratory measurements indicate 15-20% energy loss during large ELM events in DIII-D [1], and we note that the numerical simulation has not completed the ELM cycle. The internal energy is still decreasing at the end of the simulation while pressure is lost over the entire pedestal region. The computation finds that the primary loss channel

is convective (n**T**$\mathbf{V}$) rather than conductive ($\mathbf{q}$), which is not inconsistent with laboratory measurements [1].

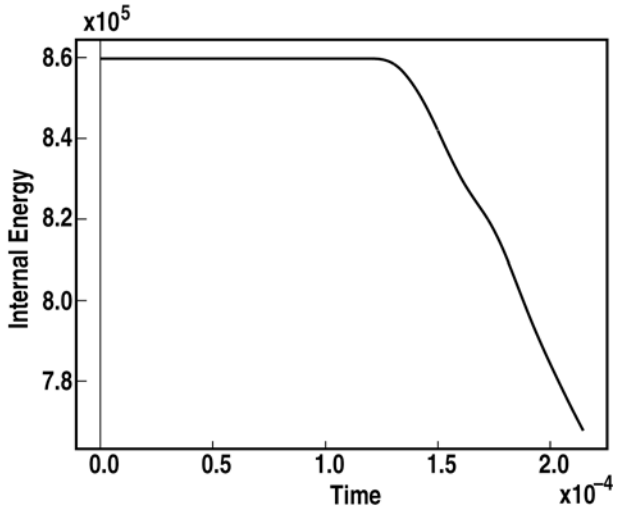

Fig. 11. As a result of the nonlinear evolution of the ELM activity, approximately 10% of the internal energy is lost within 60 μs.

4. DISCUSSION AND SUMMARY

Because of the deleterious effects of ELMs on plasma performance and operation, it is important to understand both their onset and the manner in which they deposit heat on the wall. A better understanding of onset will lead to operations and control techniques that avoid the most harmful form of ELMs. Knowledge of heat transport can be used to engineer configurations that are robust to ELM activity.

The linear studies in this report represent the first significant parameter scan to consider the effects of a separatrix and collisionality on ELMs. At present, the results must be considered preliminary, since more numerical convergence testing is needed. The results are sufficiently mature, however, to provide a useful guide for the requirements of nonlinear simulations. The nonlinear simulation presented here is the first to show significant plasma-wall interactions as a result of an ELM instability over a global computational domain. While the nonlinear simulation is also preliminary in many ways, it appears to reproduce some important experimental observations such as the energy loss time-scale and the heat loss mechanism. This suggests that nonlinear fluid simulations have potential to provide insight into how ELMs evolve and deposit heat onto the wall. Further refinements of the simulations will include more accurate geometry, improved boundary conditions, and more refined physics models, such as non-linear two-fluid and gyro-viscous effects.

REFERENCES

[1] M.R. Wade, K.H. Burrell, J.T. Hogan, *et al*., Phys. Plasmas **12**, 056120 (2005).

[2] C.R. Sovinec, A.H. Glasser, D.C. Barnes, *et al*., J. Comput. Phys. **195**, 355 (2004).

[3] P.B. Snyder, H.R. Wilson, J.R. Ferron, *et al.,* Phys. Plasmas **9**, 2037 (2002).

[4] H.R. Wilson, P.B. Snyder, G.T.A. Huysmans and R.L. Miller, Phys. Plasmas **9**, 1277 (2002).

[5] P. B. Snyder, H. R. Wilson and X. Q. Xu, Phys. Plasmas **12**, 056115 (2005).

[6] C.R. Sovinec, D.D. Schnack, A.Y. Pankin, *et al.,* J. Physics: Conference Series **16**, (2005).

[7] E.D. Held, J.D. Callen, C.C. Hegna, *et al.,* Phys. Plasmas **11**, 2419 (2004).

[8] S.E. Kruger, D.D. Schnack and C.R. Sovinec, Phys. Plasmas **12**, 056113 (2005).

ACKNOWLEDGMENT

This work was supported by the U.S. Department of Energy under and DE-FG02-95ER54309 and DE-FG02-92ER54139.